

FAST TRACK COMMUNICATION

Contrasting characteristics of sub-microsecond pulsed atmospheric air and atmospheric pressure helium–oxygen glow discharges

J L Walsh¹, D X Liu^{1,2}, F Iza¹, M Z Rong² and M G Kong^{1,3}¹ Department of Electronic and Electrical Engineering, Loughborough University, Leics LE11 3TU, UK² State Key Lab of Electrical Insulation and Power Equipments, Xi'an Jiaotong University, 710049, People's Republic of ChinaE-mail: m.g.kong@lboro.ac.uk

Received 23 September 2009, in final form 12 November 2009

Published 8 January 2010

Online at stacks.iop.org/JPhysD/43/032001**Abstract**

Glow discharges in air are often considered to be the ultimate low-temperature atmospheric pressure plasmas for numerous chamber-free applications. This is due to the ubiquitous presence of air and the perceived abundance of reactive oxygen and nitrogen species in air plasmas. In this paper, sub-microsecond pulsed atmospheric air plasmas are shown to produce a low concentration of excited oxygen atoms but an abundance of excited nitrogen species, UV photons and ozone molecules. This contrasts sharply with the efficient production of excited oxygen atoms in comparable helium–oxygen discharges. Relevant reaction chemistry analysed with a global model suggests that collisional excitation of O₂ by helium metastables is significantly more efficient than electron dissociative excitation of O₂, electron excitation of O and ion–ion recombination. These results suggest different practical uses of the two oxygen-containing atmospheric discharges, with air plasmas being well suited for nitrogen and UV based chemistry and He–O₂ plasmas for excited atomic oxygen based chemistry.

(Some figures in this article are in colour only in the electronic version)

Non-equilibrium atmospheric pressure plasmas are becoming increasingly important in industrial and biomedical applications due to the scope and diversity of their reaction chemistry at low gas temperatures without the need for a vacuum chamber [1, 2]. In low pressure discharges, ions tend to be highly energetic, hence many low pressure processing applications are driven by ion bombardment, such as semiconductor wafer processing [3]. At atmospheric pressures, where collisions occur on a picosecond timescale and the mean free path is on a tens of nanometres scale, it is difficult to accelerate ions to the energies required to trigger ion-enabled surface chemistry [4].

Consequently, applications employing atmospheric plasmas tend to be driven by a high flux of reactive chemical species such as atomic O, O₃, OH, NO and others [2, 5, 7]. Detailed understanding of reaction chemistry in atmospheric discharges is essential to achieve optimum application efficacy and processing control. The need to maximize the flux of reactive species produced must be balanced out by the need to maintain plasma stability. This is challenging for atmospheric plasmas and is often approached by employing a noble base gas (e.g. helium or argon) mixed with a small admixture of a reactive precursor gas such as oxygen [5–8]. For practical applications where process economy is important, it is always attractive to use less costly molecular gases, for example air. The

³ Author to whom any correspondence should be addressed.

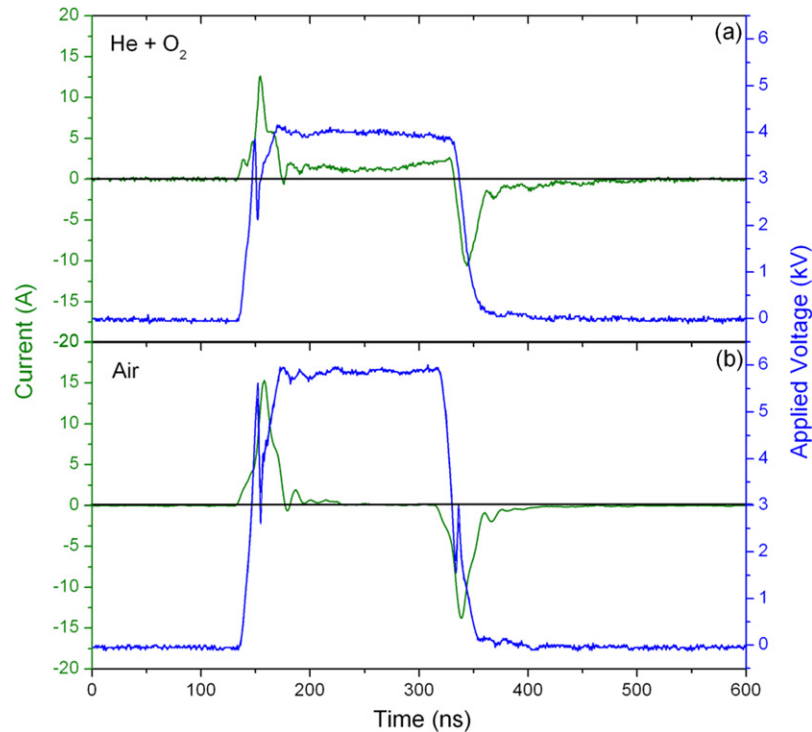


Figure 1. Current and voltage waveforms obtained in the pulsed atmospheric dielectric-barrier discharge operating in (a) helium with 0.5% oxygen admixture and (b) ambient air.

usual tendency for atmospheric air discharges to evolve into a hot filamentary plasma can be controlled effectively by using, for example, sub-microsecond pulsed excitation [9–11] and micrometre-scale discharge geometry [12, 13].

While it is possible to generate stable and low-temperature atmospheric air plasmas, it is not clear whether they offer appropriate reaction chemistry. This study compares the production of key reactive species and UV photons in two oxygen-containing atmospheric plasmas, namely a pulsed helium–oxygen discharge and a pulsed air discharge. In all experiments detailed here, the electrode unit consisted of two cylindrical steel electrodes with a 2 mm separation, the electrode area was 7 cm² and a 1 mm thick Al₂O₃ sheet covered one electrode thus reducing the gas gap to 1 mm. The electrode unit was housed in an enclosure into which air was fed at a rate of 5 standard litres per minute (SLM). In the He–O₂ case, the total gas flow was fixed at 5 SLM with an adjustable O₂/He ratio nominally at 0.5% that was found to achieve an optimal inactivation of bacteria [14] and biomolecules [5]. A home-made high voltage pulse generator delivered pulses up to 15 kV in magnitude and ~200 ns FWHM duration to the dielectric covered electrode at 5 kHz. The average dissipated power was calculated by integrating the instantaneous power over a single pulse and multiplying by the repetition frequency. This was done in real time allowing the power dissipation in the plasma to be monitored *in situ*. A fibre optic cable and collimating lens were fixed 5 mm from the discharge edge to allow optical diagnostics to be conducted. To support the experimental study, a global model of He–O₂ plasmas was developed. Similar global models have been widely used for analysing capacitively coupled discharges

both at low and atmospheric pressure [15, 16]. As global models are computationally simple, it is possible to implement a large number of reactions and species to realistically model complex discharge chemistry. The global model employed here accounts for 18 species, including e, He*, He₂*, He⁺, He₂⁺, O(¹D), O(¹S), O, O₂(a), O₂(b), O⁺, O₂⁺, O⁻, O₂⁻, O₃ and O₃⁻, contributing to 206 reactions. The input parameters are dissipated power, gas temperature and densities of ground state He and O₂. For a given power, the particle and power balance equations are solved simultaneously to determine the steady-state plasma composition [15].

Using the 200 ns voltage pulses with rise and fall times of <20 ns, both pulsed atmospheric discharges were found to be stable and free from streamers. Figure 1 depicts their measured current and voltage waveforms with O₂/He = 0.5% for the He–O₂ plasma. While the temporal characters of their electrical signals are similar, the peak voltage of the air plasma is higher at 5.9 kV than 4 kV of the He–O₂ plasma. Its currents are also larger at 15 A and –14 A associated with the rising and falling edges of the voltage, respectively, compared with 12.6 A and 10 A in the He–O₂ plasma. These would suggest a more intense discharge in the air plasma. However, the average dissipated power in both discharges was found to be very similar at ~3 W. Further analysis uncovered that the He–O₂ plasma consumed 65% of the total power dissipated during the 200 ns pulse duration with the remaining 35% occurring at the voltage rising and falling edges. In contrast, only 10% of the power in the air discharge was dissipated during the voltage pulse of 200 ns. Close inspection of figure 1(a) reveals a dc current component of ~2 A throughout the duration of the voltage pulse. This dc current may be related to the drift of

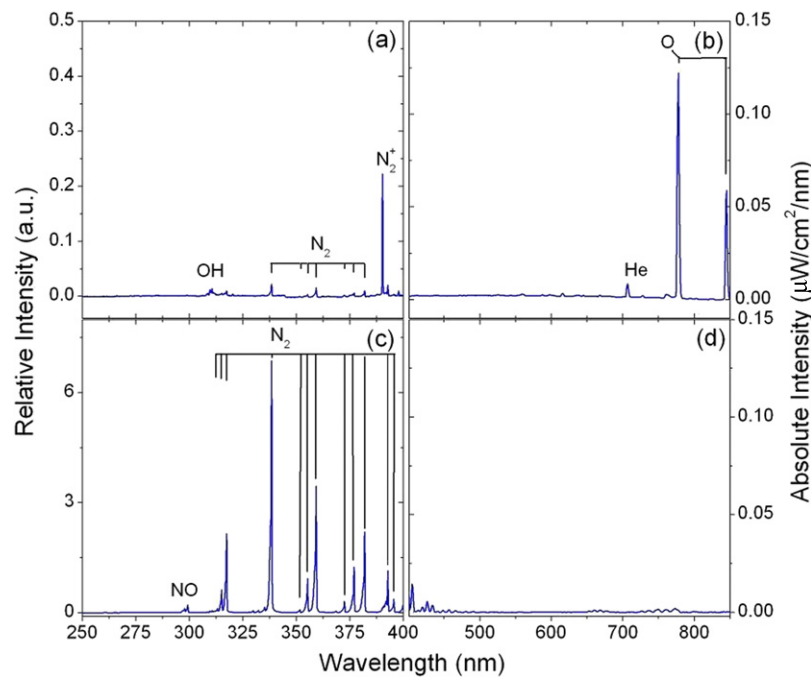


Figure 2. Relative (a) and absolute (b) emission spectra of the pulsed He + O₂ plasma at O₂/He = 0.5% and relative (c) and absolute (d) emission spectra of the pulsed air discharge, both operating at 3 W.

electrons generated via Penning ionization of nitrogen impurity ($\epsilon_{iz} \sim 15$ eV) in the helium gas by atomic and molecular helium metastables, (He(2^3S) 19.8 eV, He(2^1S) 20.6 eV and He $_2^*$ 18.4 eV) [17]. These helium species are obviously absent in the air discharge, whereas other metastables such as nitrogen and oxygen do not have sufficient energy to ionize the background gas, O(1D) 1.97 eV, O $_2^*$ ($^1\Delta_g$) 0.98 eV, N $_2$ ($A^3\Sigma_u^+$) 6.22 eV and N $_2$ ($C^3\Pi_u$) 11.05 eV [18].

The relative emission spectra of the UV band (250–400 nm) shown in figures 2(a) and (c) were obtained using a 1200 grooves mm⁻¹ grating to give a spectral resolution of ~ 0.1 nm. The absolute emission spectra of the visible spectrum (400–850 nm) in figures 2(b) and (d) were measured with a 150 grooves mm⁻¹ grating that provided a ~ 2 nm resolution. Emission spectra from the He–O₂ discharge are dominated by excited atomic oxygen, O(5P) and O(3P) at 777 nm and 845 nm, respectively. Helium, nitrogen and OH species are also observed but at a lower intensity. Emission from the second positive system of N $_2$ is significantly lower than N $_2^+$ ($B^2\Sigma_g^+$) emission at 391 nm. N $_2^+$ ($B^2\Sigma_g^+$) is readily produced through, among other routes, Penning ionization by helium metastables [17, 19, 20]. This supports the explanation for the dc current in figure 1(a) that it is likely due to electrons produced via Penning processes. Despite the far higher concentration of He than O₂ in the background gas, He emission at 706 nm ($^3S_1 - ^3P_1$) is significantly lower than atomic oxygen emission at 777 and 845 nm. This has been reported in other atmospheric helium discharges [17, 20–22], and is attributed to different excitation mechanisms [20].

For the air plasma, there is strong emission from nitrogen species below 400 nm, most notably the nitrogen second positive system, but also from nitric oxide. In comparison with the He–O₂ discharge, the N $_2$ second positive emission of

the air plasma is notably larger and OH emission is absent. High nitrogen emission in the air plasma is likely due to the far higher N $_2$ concentration than in the He–O₂ mixture. However N $_2^+$ ($B^2\Sigma_g^+$) emission is comparable in the two discharges. In a He–O₂ plasma with a small N $_2$ density as impurity, Penning reactions involving He metastables contribute significantly to N $_2^+$ ($B^2\Sigma_g^+$) emission and are likely to account for comparable 391 nm emission in the two plasmas. The most striking difference in figure 2 is that the air plasma produces very little emission above 400 nm where many reactive oxygen emission lines exist. In particular, there is little emission at the atomic oxygen lines of 777 and 845 nm. This contrast in excited atomic oxygen is significant for bacterial and biomolecule inactivation [5, 23] and will be discussed further with simulation data.

Gas temperature has direct implications for many applications and influences plasma chemistry. The contrast in excited atomic oxygen of the two oxygen-containing plasmas indicated in figure 2 may be influenced by a difference in their gas temperature. Molecular gas discharges, particularly in air, are known to have elevated temperatures when compared with noble gas discharges in helium and argon. Typically, this is because air discharges require substantially higher power densities than noble gas discharges particularly when driven by continuous-wave excitation. The effect of short-pulsed excitation, however, acts to reduce the amount of power needed to sustain the discharge [24], and its long off-time allows significant gas cooling between consecutive pulses leading to a lower gas temperature. As a result, the average dissipated power densities in sub-microsecond pulsed discharges are considerably reduced to 2–10 W cm⁻³ regardless of the gas used [10, 21]. Figure 3 highlights the rotational temperature of nitrogen at a constant dissipated power of 3 W in the

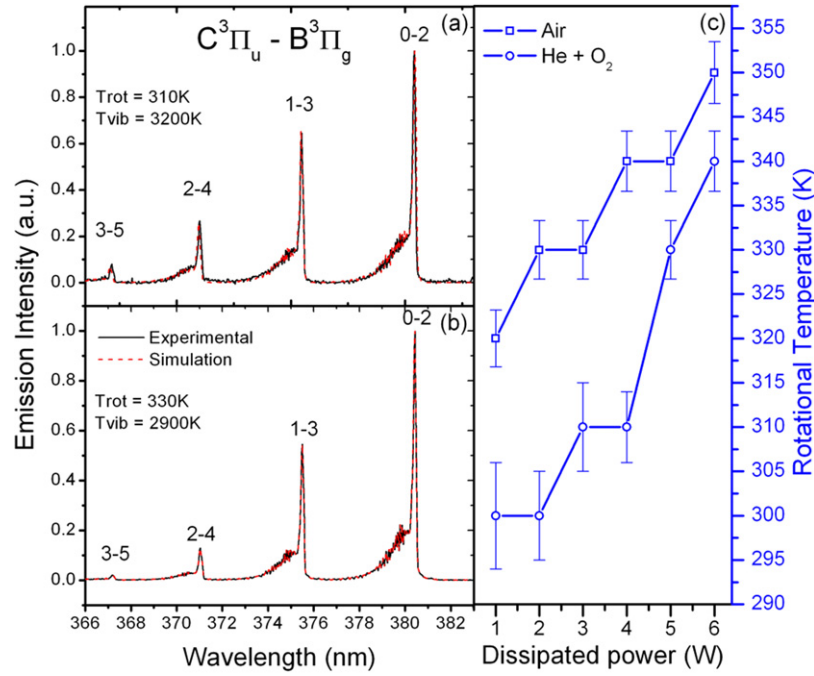


Figure 3. Experimental and simulated best-fit data of the second positive nitrogen emission band for (a) the He–O₂ plasma and (b) the air plasma, both at 3 W of dissipated power, with the power dependence of the rotational temperature in (c).

two discharges, obtained from Specair assuming that nitrogen rotational and translational temperatures are in equilibrium. Figures 3(a) and (b) suggest that $T_{\text{rot}} = 310$ K in the He–O₂ discharge and $T_{\text{rot}} = 330$ K in the air discharge. As expected, the air discharge has a slightly higher gas temperature; however, the fitting errors are found to be up to ± 10 K. Consequently the gas temperature in both discharges can be considered to be similar and is unlikely to contribute to the contrast in excited O emission. Figure 3(c) shows that T_{rot} of the He–O₂ plasma changes from 300 to 340 K between 1 and 6 W, whereas the temperature in the air plasma increases from 330 to 350 K when the power is increased from 2 to 6 W. The rate of change in temperature is greater in the He–O₂ plasma, and this is attributed to the heating by the dc current component during the voltage pulse.

Figures 4(a) and (b) show the excited oxygen emission intensity and ozone concentration from each discharge as a function of input power. Figure 4(a) shows the trend in emission intensity of atomic oxygen, O(⁵P) at 777 nm and O(³P) at 845 nm, for both the air and helium–oxygen discharges. At 3 W, the emission intensity of excited atomic oxygen in the He–O₂ plasma is a factor of 85 and 180 at 777 nm and 845 nm, respectively, higher than in the air plasma. An increase in dissipated power yields an increase in emission intensity of both species, as a higher dissipated power yields a higher electron density which in turn produces a higher density of species. For ozone concentration shown in figure 4(b), each measurement was taken 20 s after igniting the discharge, a Gastec ozone sampling tube (18M 2–200 ppm range) was placed at the exhaust of the discharge chamber and a sample was drawn from the exhaust gas. As ozone takes a significant time to decompose back to oxygen, it was necessary to flush the enclosure with the base gas for several minutes after each

measurement was taken to remove any residual ozone. Similar to the O trend in figure 4(a), ozone production is proportional to the dissipated power. In the air plasma, the ozone levels increase from 70 ppm at 2 W to 170 ppm at 6 W, comparable to those reported in similar atmospheric discharges [25]. In the He–O₂ plasma, the ozone density increases from 15 ppm at 1 W to 95 ppm at 6 W when O₂/He = 0.5%. Also shown is the ozone concentration for O₂/He = 1% and 1.5% at a constant power of 6 W, suggesting an ozone increase by roughly 50 ppm for every 0.5% of oxygen added to the base gas.

To help with the interpretation of figure 4, key reactions in the two O₂-containing plasmas are analysed. For the air plasma, air is assumed to consist of only N₂ and O₂ as impurities such as Ar, CO₂ and water vapour were absent from figure 2. Table 1 highlights the main pathways responsible for O(³P) and O(⁵P) population and depopulation in a He–O₂ discharge and figure 5 shows relative contributions of these mechanisms calculated from the He + O₂ global model. The steady-state electron temperature is found to be ~ 2.5 eV. Pathways 1 and 2 (table 1) involve electron excitation of O₂ and O, respectively. While the rate coefficient in pathway 2 is ~ 100 times higher than that in pathway 1, the density ratio of [O]/[O₂] is approximately 10^{-3} meaning pathway 1 dominates over pathway 2 [26]. Collisional excitation by He metastables is found to be extremely efficient for O(³P) and O(⁵P) production. This is in spite of rate coefficients for collisional excitation to O(³P) and O(⁵P) by helium metastables being estimated conservatively at 10^{-12} cm³ s⁻¹ here, based on the reported total rate for He* + O₂ of 2.4×10^{-10} cm³ s⁻¹ [27]. As previously reported [20], oxygen emission in the presence of nitrogen is not time modulated, suggesting that electron excitation reactions are unlikely to be significant in the population of O(³P) and O(⁵P). Ion–ion recombination is

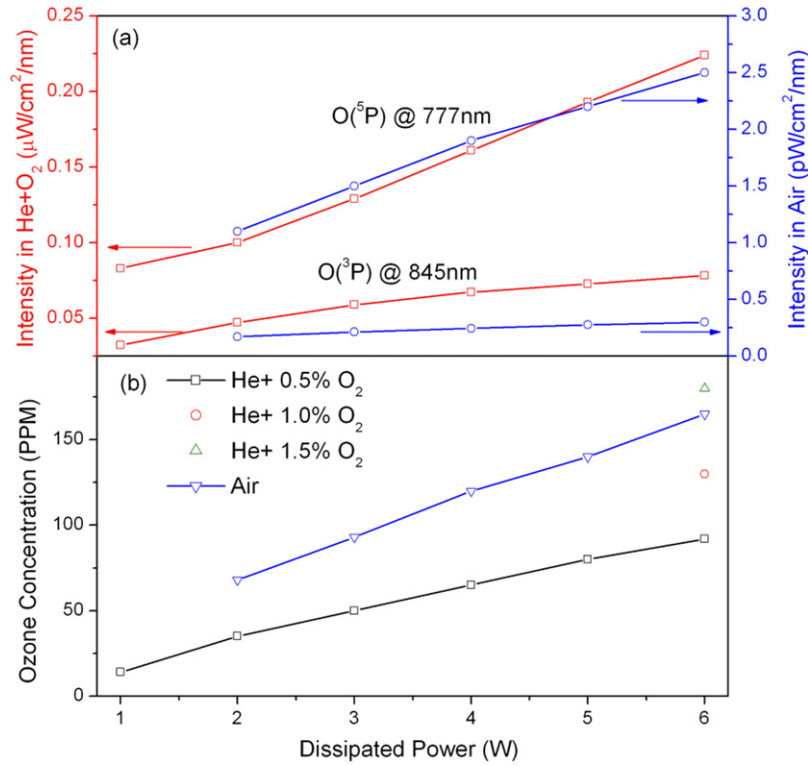


Figure 4. Dissipated power dependence of (a) the absolute emission intensity of $O(^5P)$ at 777 nm and $O(^3P)$ at 845 nm and (b) ozone concentration for the air and the He– O_2 plasma. In the He– O_2 plasma, O_2/He is (a) 0.5% and (b) 0.5, 1.0 and 1.5%.

Table 1. Key reactions and their rate coefficients used in the He– O_2 global model.

	Reaction	Rate ($\text{cm}^{-3} \text{s}^{-1}$)	Reference
Path 1	$e + O_2 \rightarrow O(3p^3P) + O + e$	$1.51 \times 10^{-10} T_e^{0.5} \exp(-16.1/T_e)$	[26]
	$e + O_2 \rightarrow O(3p^5P) + O + e$	$2.89 \times 10^{-10} T_e^{0.5} \exp(-15.9/T_e)$	[26]
Path 2	$e + O \rightarrow O(3p^3P) + e$	$3.23 \times 10^{-9} T_e^{-0.2} \exp(-10.98/T_e)$	[26]
	$e + O \rightarrow O(3p^5P) + e$	$1.51 \times 10^{-9} T_e^{-0.45} \exp(-10.73/T_e)$	[26]
Path 3	$He^* + O_2 \rightarrow O + O(3p^3P) + He$	1×10^{-12}	[27]
	$He^* + O_2 \rightarrow O + O(3p^5P) + He$		
	$He_2^* + O_2 \rightarrow O + O(3p^3P) + 2He$		
	$He_2^* + O_2 \rightarrow O + O(3p^5P) + 2He$		
Path 4	$O^+ + O^- \rightarrow O(3p^3P) + O$	1×10^{-9}	Estimated from [28, 29]
	$O^+ + O^- \rightarrow O(3p^5P) + O$		
	$O_2^+ + O^- \rightarrow O(3p^3P) + O_2$		
	$O_2^+ + O^- \rightarrow O(3p^5P) + O_2$		
	$O^+ + O_2^- \rightarrow O(3p^3P) + O_2$		
	$O^+ + O_2^- \rightarrow O(3p^5P) + O_2$		
Path 5	$O(3p^3P) \rightarrow O(3s^3S) + h\nu$	3.22×10^7	[30]
	$O(3p^5P) \rightarrow O(3s^5S) + h\nu$	3.69×10^7	[30]
Path 6	$O(3p^3P) + He \rightarrow O + He$	7×10^{-12}	[22]
	$O(3p^5P) + He \rightarrow O + He$	7×10^{-12}	Assumed the same as for $O(^3P)$
	$O(3p^3P) + O_2 \rightarrow O + O_2$	7.4×10^{-10}	[26]
	$O(3p^5P) + O_2 \rightarrow O + O_2$	1×10^{-9}	[26]

another possible population pathway. The simulation results indicate that O_2^+ is the dominant ion while O^- and O_2^- are the dominant anions. Their recombination rates are about three orders of magnitude higher than for pathway 3; however, the density ratio of $[O^- + O_2^-]/[O_2]$ is 10^{-6} . As a result, ion–ion recombination is not an efficient population mechanism of $O(^3P)$ and $O(^5P)$. Depopulation of $O(^3P)$ and $O(^5P)$ occurs via radiation (pathway 5) and quenching (pathway 6). The quenching rate is found to be $2.88 \times 10^8 \text{ s}^{-1}$, and the rate

ratio from quenching to radiation is 9 : 1. Radiative processes, however, are still significant.

In the atmospheric air discharge, similar population processes are expected [18] except for those involving helium metastables (e.g. pathway 3). Other metastable states, such as nitrogen, do not have sufficient energy to cause collisional excitation of oxygen. In addition, electron excitation of O_2 and O is expected to be inefficient due to the electronegative nature (i.e. low electron density) in low-temperature ($<1000 \text{ K}$) air

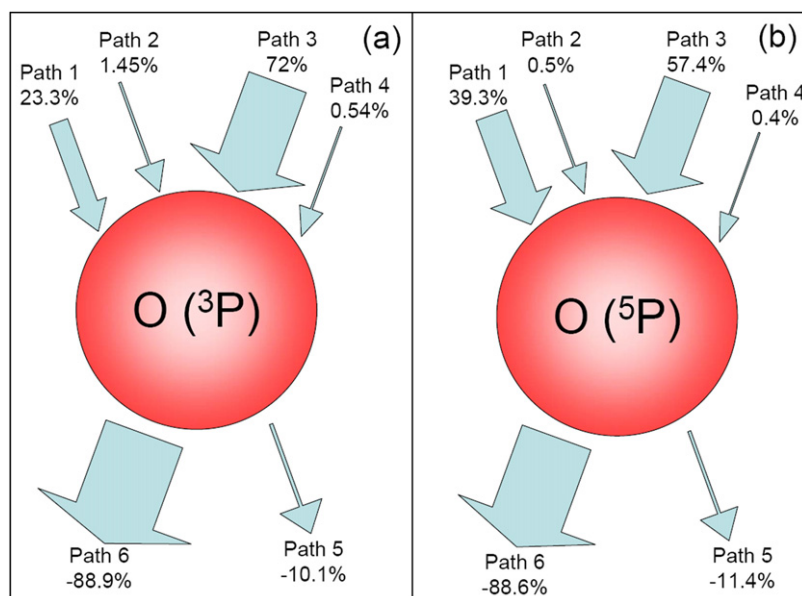


Figure 5. Schematic representation of the He–O₂ global model results showing key reaction pathways responsible for populating and depopulating (a) O(³P) and (b) O(⁵P) at 6 W of dissipated power. Percentages indicate their relative contributions.

plasmas [18]. Ion–ion recombination is also inefficient in air discharges at low temperatures (<1000 K) due to the very low density of O₂⁺ [18]. On the other hand, the main depopulation process of O(³P) and O(⁵P) in the air plasma is quenching with N₂ and O₂. Reference [31] suggests that the quenching rate coefficient via nitrogen is $4.2 \times 10^{-10} \text{ cm}^3 \text{ s}^{-1}$, leading to a quenching rate of $1.31 \times 10^{10} \text{ s}^{-1}$ in the air plasma. This indicates a rate ratio from quenching to radiation of about 400:1 in the air plasma, so radiative decay contributes far less to the depopulation rate. In comparison with the He–O₂ plasma, the depopulation of excited atomic oxygen is about ~45 times higher in the air plasma. In short, population of O(³P) and O(⁵P) in a He + O₂ discharge is significantly more efficient than in an air discharge and its quenching is significantly slower. As a result very little atomic oxygen emission is observed in air discharges when compared with He + O₂ plasmas.

For atmospheric pressure discharges, particularly in molecular gases, short-pulse excitation is critical to attain low gas temperature and robust plasma stability compared with the common sinusoidal excitation [25, 32, 33]. In general, the extent of these benefits depends on pulsewidth [21, 34–36], pulse rise and fall times [34, 37] and pulse repetition frequency [21, 34, 38]. Similar to most high-pressure short-pulsed plasmas, the sub-microsecond pulsed atmospheric plasmas reported here employ a dielectric-barrier configuration and the use of dielectric barriers results in typically two current pulses for every voltage pulse (see figure 1). Typically, discharge current is observed during the voltage rising and falling phases with very little current flow during the applied voltage. When the pulsewidth of the applied voltage was increased from 200 ns in the case of figures 1–4, the two current pulses produced during one voltage pulse were moved further apart by the increased pulsewidth of the applied voltage. With the averaged dissipated power maintained at 3 W, the gas temperature was relatively independent of the voltage

pulsewidth in our experiments. For example at a voltage pulse of 1 μs and a dissipated power of 3 W, the gas temperature was found to be 340 K and 330 K for the pulsed atmospheric air and atmospheric He–O₂ plasmas, respectively. With an error bar of ±10 K, these are similar to 330 K and 310 K for the air and He–O₂ plasmas, respectively, when the voltage pulsewidth was 200 ns (see figure 3). The larger temperature increase in the He–O₂ case is due to the small dc component in its discharge current (see figure 1(a)). It should be emphasized, however, that in the He–O₂ case both the applied voltage and the discharge current had to be reduced considerably to maintain the same averaged dissipated power of 3 W when the voltage pulsewidth was increased to 1 μs from 200 ns. If the applied voltage is allowed to increase, the averaged dissipated power would increase and the gas temperature would also increase. For our experiments, the benefits of pulsed excitation in terms of low gas temperature and large reactive species concentrations would start to diminish after the voltage pulsewidth is much above 100 μs and the rise time is above 10 μs. This suggests an interesting correlation between the gas temperature and the averaged dissipated power in two different gases.

More importantly, however, shorter pulsewidth allows for the use of much elevated applied voltage (hence larger reduced electric field of E/N) to induce larger peak discharge current (hence higher electron density), both desirable for active plasma chemistry. In fact, the use of sub-microsecond and even nanosecond pulsed excitation would facilitate the possibility to manipulate the electron energy distribution function and in turn manipulate plasma chemistry [37]. This study has not addressed directly the effect of pulse rise time and pulse repetition frequency. However, it is known that shorter rise time would permit the use of over-voltage and the resulting increase in E/N would lead to more abundant reactive species and UV emission [34]. It is also known that higher repetition frequency would in general increase the production of reactive

plasma species [21] though the relationship is not always monotonic [38]. It is important to remark that the use of short pulses not only reduces the gas temperature but also enables access to active and diverse plasma chemistry that cannot be easily accessed using sinusoidal excitation. Finally it is worth mentioning that sub-microsecond pulsed atmospheric plasmas were achieved in helium without dielectric barriers with one current pulse every voltage pulse [21, 37, 39], suggesting a different plasma generation mechanism.

In conclusion, this paper has presented a study of two atmospheric oxygen-containing discharges. Using sub-microsecond pulses, the gas temperature was low and similar in both cases. Of particular note is that the atomic oxygen emission intensity was about two orders of magnitude higher in the He–O₂ discharge compared with that observed in the air plasma. A global model for He–O₂ plasmas was used to establish that production of excited oxygen atoms is more efficient in the He–O₂ plasma than in the air plasma. Furthermore, quenching of O(³P) and O(⁵P) in the air plasma was found to be ~45 times higher than in the He–O₂ discharge. These two findings explain the contrast in excited O emission and suggest that the two oxygen-containing atmospheric discharges may have different uses, with air plasmas being well suited for applications requiring nitrogen and UV based chemistry and He–O₂ plasmas for those requiring excited atomic oxygen.

References

- [1] Iza F, Kim G J, Lee S M, Lee J K, Walsh J L, Zhang Y T and Kong M G 2008 *Plasma Process. Polym.* **5** 322
- [2] Fridman G, Friedman G, Gutsol A, Shekhter A B, Vasilets V N and Fridman A 2008 *Plasma Process. Polym.* **5** 503
- [3] Graves D B 1994 *IEEE Trans. Plasma Sci.* **22** 31
- [4] Iza F, Lee J K and Kong M G 2007 *Phys. Rev. Lett.* **99** 075004
- [5] Deng X T, Shi J J and Kong M G 2007 *J. Appl. Phys.* **101** 074701
- [6] Walsh J W and Kong M G 2008 *Appl. Phys. Lett.* **93** 111501
- [7] Shimizu T *et al* 2008 *Plasma Process. Polym.* **5** 577
- [8] Walsh J W and Kong M G 2008 *Appl. Phys. Lett.* **91** 221502
- [9] Pancheshnyi S V, Lacoste D A, Bourdon A and Laux C O 2006 *IEEE Trans. Plasma Sci.* **34** 2478
- [10] Walsh J L and Kong M G 2007 *Appl. Phys. Lett.* **91** 251504
- [11] Ayan H, Staack D, Fridman G, Gutsol A, Mukhin Y, Starikovskii A, Fridman A and Friedman G 2007 *J. Phys. D: Appl. Phys.* **42** 125202
- [12] Hopwood J and Iza F 2004 *J. Anal. At. Spectrom.* **19** 1145
- [13] Kolb J F, Mohamed A H, Price R O, Swanson R J, Bowman A, Chiavarini R L, Stacey M and Schoenbach K H 2008 *Appl. Phys. Lett.* **92** 241501
- [14] Yu H, Perni S, Shi J J, Wang D Z, Kong M G and Shama G 2006 *J. Appl. Microbiol.* **101** 1323
- [15] Kim S, Lieberman M A, Lichtenberg A J and Gudmundsson J T 2006 *J. Vac. Sci. Technol. A* **24** 2025
- [16] Stalder K R, Vidmar R J, Nersisyan G and Graham W G 2006 *J. Appl. Phys.* **99** 093301
- [17] Nersisyan G, Morrow T and Graham W G 2004 *Appl. Phys. Lett.* **85** 1487
- [18] Becker K H, Kogelschatz U, Schoenbach K H and Baker R J 2005 *Non-Equilibrium Air Plasmas at Atmospheric Pressure* (Bristol: Institute of Physics Publishing) ISBN 0 7503 0962 8
- [19] Sublet A, Ding C, Dorier J, Hollenstein C, Fayet P and Coursimault F 2006 *Plasma Sources Sci. Technol.* **15** 627
- [20] Liu D W, Iza F and Kong M G 2009 *Appl. Phys. Lett.* **95** 031501
- [21] Walsh J L and Kong M G 2006 *Appl. Phys. Lett.* **89** 231503
- [22] Niemi K, Schulz-von der Gathen V and Doebele H F 2001 *J. Phys. D: Appl. Phys.* **34** 2330
- [23] Perni S, Shama G, Hobman J L, Lund P A, Kershaw C J, Hidalgo-Arroyo G A, Penn C W, Deng X T, Walsh J L and Kong M G 2007 *Appl. Phys. Lett.* **90** 073902
- [24] Walsh J L, Shi J J and Kong M G 2006 *Appl. Phys. Lett.* **88** 171501
- [25] Williamson J M, Thump D D, Bletzing P and Ganguly B N 2006 *J. Phys. D: Appl. Phys.* **39** 4400
- [26] Pagnon D, Amorim J, Nahorny J, Touzeau M and Vialle M 1995 *J. Phys. D: Appl. Phys.* **28** 1856
- [27] Leveille V and Coulombe S 2006 *Plasma Process. Polym.* **3** 587
- [28] Ishikawa T, Hayashi D, Sasaki K and Kadota K 1998 *Appl. Phys. Lett.* **72** 2391
- [29] Zhou X X and Dickson A S 1997 *Nucl. Instrum. Methods Phys. Res. B* **124** 51
- [30] Ralchenko Yu, Kramida A E, Reader J and NIST ASD Team 2008 *NIST Atomic Spectra Database* (version 3.1.5)
- [31] Gordiets B F, Ferreira C M, Guerra V L, Loureiro J M A, Nahorny J, Pagnon D, Touzeau M and Vialle M 1995 *IEEE Trans. Plasma Sci.* **23** 750
- [32] Mildren R P and Carman R J 2001 *J. Phys. D: Appl. Phys.* **34** L1
- [33] Kong M G and Deng X T 2003 *IEEE Trans. Plasma Sci.* **31** 7
- [34] Leiweke R J and Ganguly B N 2007 *Appl. Phys. Lett.* **90** 241501
- [35] Lu X, Xiong Q, Xiong Z, Xian Y, Zhou F, Hu J, Gong W, Zhou C, Tang Z, Jiang Z and Pan Y 2009 *IEEE Trans. Plasma Sci.* **37** 647
- [36] Panousis E, Merbahi N, Clément F, Ricard A, Yousfi M, Papageorghiou L, Loiseau J F, Eichwald O, Held B and Spyrou N 2009 *IEEE Trans. Plasma Sci.* **37** 1004
- [37] Iza F, Walsh J W and Kong M G 2008 *IEEE Trans. Plasma Sci.* **37** 1289
- [38] Carman R J, Mildren R P, Ward B K and Kane D M 2004 *J. Phys. D: Appl. Phys.* **37** 2399
- [39] Walsh J W and Kong M G 2006 *Appl. Phys. Lett.* **89** 161505